6-1-2017

Quasistatic Error Modeling and Model Testing for a 5-Axis Machine

H-W. Ko

P. Bazzoli

Jared Adam Nisbett

L. Ma

et. al. For a complete list of authors, see http://scholarsmine.mst.edu/mec_aereng_facwork/3733

Recommended Citation

H. Ko et al., "Quasistatic Error Modeling and Model Testing for a 5-Axis Machine," *Procedia Manufacturing*, vol. 10, pp. 443-455, Elsevier, Jun 2017.
The definitive version is available at https://doi.org/10.1016/j.promfg.2017.07.023

Available online at www.sciencedirect.com

ScienceDirect

Procedia Manufacturing 10 (2017) 443 – 455

Procedia MANUFACTURING

45th SME North American Manufacturing Research Conference, NAMRC 45, LA, USA

Quasistatic Error Modeling and Model Testing for a 5-Axis Machine

Hua-Wei Ko[a], Patrick Bazzoli[b], J. Adam Nisbett[b], Le Ma[b], Douglas Bristow[b], Robert G. Landers[b], Yujie Chen[c], Shiv G. Kapoor[a] and Placid M. Ferreira[a,*]

[a]*Mechanical Science and Engineering, University of Illinois at Urbana-Champaign, Urbana, IL, 61801, USA*
[b]*Department of Mechanical and Aerospace Engineering, Missouri University of Science and Technology, Rolla, MO 65409,USA*
[c]*Innovation and Technology Development Division (ITDD), Caterpillar Inc. Peoria, IL.*

Abstract

This paper presents an approach to modeling the quasistatic errors of a 5-axis machine tool with one redundant axis. By introducing errors to the ideal joints and shape transforms of the kinematics of the machine, an error model is obtained. First order error characteristics are used to parameterize the introduced errors. It is found that of the 52 introduced error parameters, only 32 have a linearly independent effect on the volumetric errors observed in the machine's workspace. To identify these error parameters, the volumetric error components at 290 randomly chosen points are measured with a laser tracker. The unknown parameters are obtained by least-squares estimation, and the resulting model able to reduce average magnitude of the volumetric error vectors at these points by an average of 90% of their original values. Further, the identified model was used to predict the errors observed in two independent test point sets (each set consisting of 48 points). A 75% reduction in the average magnitude of the error vectors was observed. A large fraction of the residual errors was found to be attributable to the thermal drift of the machine during the experiments where were not conducted in a thermally controlled environment and the positioning repeatability of the machine.

Peer-review under responsibility of the organizing committee of the 45th SME North American Manufacturing Research Conference

Keywords: machine-tools; quasistatic machine-tool errors; machine-tool accuracy; error compensation

* Corresponding author. Tel.: +1-271-333-0639.
E-mail address: pferreir@illinois.edu

Peer-review under responsibility of the organizing committee of the 45th SME North American Manufacturing Research Conference
doi:10.1016/j.promfg.2017.07.023

1. Introduction

About 70 percent of the inaccuracy of a machine tool is caused by quasistatic errors. As their name suggest, the quasistatic errors are slowly varying errors. Quasistatic error sources include assembly errors, flexural errors (due to self-weight of moving parts and the work piece), and thermal deformations (due to heat generation at the spindle, drives, guideways and cutting tools as well as ambient temperature variations, all of which gradually generate the geometric inaccuracies in the underlying kinematic structure of the machine [1, 2]. Compared with dynamic errors (e.g., servo-tracking errors; dynamic response to cutting forces), quasistatic errors vary slowly during the operation of the machine. Due to being constrained, small thermal changes cause structural members of the machine to undergo deformation that, in turn, are magnified by the Abbe effect [5,23,24]. Therefore, thermal (drift) errors can, depending on the mode of operation and the level of control of the factory environment, become the dominant component of quasistatic errors, especially for larger machines with variable operation cycles [3-5]. For example, on a shop floor with controlled temperature and the machining operating continuously on a repeating work cycle, a thermal steady state is reached and thermal drift of the machine is minimal. However, for a machine operating in a flexible (small-batch/one-off) production setting, without shop floor temperature controls, large diurnal swings in the quasistatic errors of the machine may be observed.

Quasistatic machine-tool errors, because of their large imprint on workpiece inaccuracy, and their slow variation, are good candidates for compensation. As a result, a rich body of research exists for their characterization and compensation. A generalized predictive error model, considering combinations of polynomials and functions of nominal positions and temperature was proposed by Donmez et al. [21]. Ferreira and Liu [17] applied rigid body transformations with small error parameters to develop a linear volumetric error in workspace and used least-squares to estimate them. For machines with rotary joint, Kiridena and Ferreira [18] used perturbations to Jacobian matrix to develop error maps of different 5-axis machine configurations. On the other hand, inverse kinematics is also a common approach used to identify error components [19, 20]. Patel, Wang and Ehmann [16, 22] constructed an error model for a parallel-kinematics platform-based machine by differentiating its kinematics equations with respect to potential error sources. To model the thermally-induced error which causes the deformation of the structure of the machine to vary with time, a strategy using finite element analysis (FEA) coupled with temperature field measurements by thermocouples was proposed by Creighton, Honegger, Tulsian, and Mukhopadhyay [23]. Veldhuis and Elbestawi [24] also proposed a thermal error compensation strategy based on neural network for five-axis machine which eliminates significant error sources.

This paper builds on the modeling approach introduced by Ferreira and Liu [17] extended by Kiridena [11, 18]. First, a proper parameterization is introduced for rotary joints. Next, the approach, for the first time, is shown to work for machines with redundant axes. Finally, for the first time the approach is used in conjunction with a versatile metrology instrument such as a laser tracker [6, 7, 14, 15], allowing for a model with a large number of parameters to be identified. In this approach, the kinematic structure of the machine is modeled with shape and joint transformations [12]. Unlike the more commonly used Denavitt-Hartenberg approach [13], this modeling approach separates parameters associated with the links and the joints of the machine, allowing for avoidance of singularities and more intuitive and measurable error parameters. For CNC machines, one deals primarily with prismatic joints [1] and rotary joints [9], while the shape transformation primarily model translations across links [8]. A model for the errors of the machine is constructed by introducing small perturbations (errors) into the parameters of the shape and joint transformations and an expression for the volumetric error vector is obtained as the difference in the spatial location of the tool/spindle (relative to the workpiece table) produced by the perturbed and ideal kinematics of the machine. The equation expresses the volumetric error in terms of the yet-to-be-determined unknown perturbations of the links and joints of the machine. When observations/measurements of the volumetric errors in the machine's workspace are made, optimization techniques such as least-square fits are used to identify these perturbations [10, 11].

Section II of this paper describes the machine being considered and applied the modeling approach to it. Section III describes the model parameter identification process while Section IV deals with data collection and analysis. Section V presents statistical results on the behavior of the model identified, with Section VI draws up conclusions.

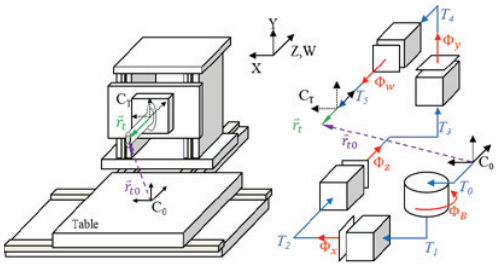

Fig. 1. Schematic of a 5-axis machine along with its kinematic model showing the shape and joint transformation.

2. Model construction

A schematic of the 5-axis machine used in this study and its kinematic equivalent are shown in Fig. 1. The travel of prismatic joints, X, Y, Z and W axis are 4m, 2.5m, 2.2m and 800mm respectively. The rotary joint, B axis allows the table to rotate about Y-axis by 360 degrees. The ideal kinematic of the machine from the table to the spindle can be expressed by the series of homogeneous transformation matrices (HTMs). This series consists of alternating joint and shape transformations. Joint transformations, denoted by Φ_i, model the constraints and degrees of freedom of the transmission elements or joints of the machine, while shape transformations model the geometry and dimensions of the structural members that hold the joints. Thus, the ideal coordinate transformation that takes a point on the tool expressed in the spindle frame to a frame attached to the table is given by:

$$H = \Phi_B T_1 \Phi_x T_2 \Phi_z T_3 \Phi_y T_4 \Phi_w T_5 \tag{1}$$

To introduce rotational and translational errors into the shape and joint transformations, constant (not position dependent) components of errors are introduced into the shape transformations while the position dependent components are introduced into the joint transformations. There are three types of transformation for a machine tool.

2.1. Shape transformation($T_1 - T_5$)

If the small dimensional (translation) and deflection (angular) errors are introduced to T_i, an ideal shape transformation, the actual transformation, shown in Fig. 2(a), becomes,

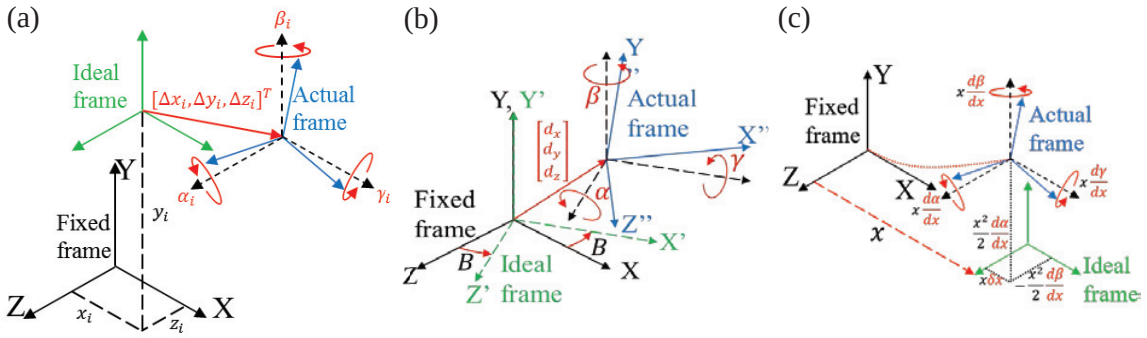

Fig. 2. (a) Ideal and actual shape transformations. The actual transform introduces small translational and rotational displacements; (b) Ideal and actual rotary joint transformations. The actual transform introduces small translational and rotational displacements to model the wandering and tilt of an actual joint; (c) Ideal and actual prismatic joint transformations. The actual transform introduces small angular motions and a positioning error to the ideal desired motion.

$$T_i' = \begin{bmatrix} 1 & -\alpha_i & \beta_i & x_i + \Delta x_i \\ \alpha_i & 1 & -\gamma_i & y_i + \Delta y_i \\ -\beta_i & \gamma_i & 1 & z_i + \Delta z_i \\ 0 & 0 & 0 & 1 \end{bmatrix}, i = 1 \sim 5, \tag{2}$$

where α_i, β_i and γ_i are small rotational errors about Z, Y and X directions, $\begin{bmatrix} x_i & y_i & z_i \end{bmatrix}^T$ and $\begin{bmatrix} \Delta x_i & \Delta y_i & \Delta z_i \end{bmatrix}^T$ are the constant shift vector and the small position errors vector in the workspace.

2.2. Rotary joint transformation(Φ_B)

The joint transformation of an ideal rotary joint (rotation about Y-axis) can be expressed as:

$$\Phi_B = \begin{bmatrix} \cos(B) & 0 & \sin(B) & 0 \\ 0 & 1 & 0 & 0 \\ -\sin(B) & 0 & \cos(B) & 0 \\ 0 & 0 & 0 & 1 \end{bmatrix}, \tag{3}$$

where B is command rotational displacement of the joint. An actual joint introduces several error motions. First, when the joint is commanded to a position B, it may have positioning error, β. Further, the rotational errors may introduce tilts of α and γ, and the entire moving table may shift due to the accumulation of translation errors d_x, d_y and d_z. Thus, as depicted in Fig. 2(b), the joint transformation for an actual rotary joint (rotation about the y-axis), assuming small angles, the errors, is given by:

$$\Phi_B' \approx \begin{bmatrix} c(B) - \beta B' sB & -\alpha B' & \mathrm{s}(B) + \beta B' \mathrm{c}(B) & B' d_x \\ \alpha B' & 1 & -\gamma B' & B' d_y \\ -\mathrm{s}(B) - \beta B' \mathrm{c}(B) & \gamma B' & \mathrm{c}(B) - \beta B' \mathrm{s}(B) & B' d_z \\ 0 & 0 & 0 & 1 \end{bmatrix}, \tag{4}$$

where $B' = \sin(B/2)$. For a typical rotary joint, for purposes of consistency one would like to have the errors at B=0° equal those at B=360°. Therefore, each of the errors (for example, α) in the transformation can be written as a summation of terms, $\alpha = \sum_{n=1}^{N} \alpha_n \sin(nB/2)$. For simplicity, only the first term is used.

2.3. Prismatic joint transformations (Φ_x, Φ_y, Φ_z and Φ_w)

An actual prismatic joint, in addition to producing the desired translation, will also produce error motions, including error in positioning along the joint, straightness errors and angular errors. As is evident for this transformation matrix, the error terms are functions of the joint displacement. A HTM of a prismatic joint, proposed by Ferreira and Liu [8] is given below:

$$\Phi_x' = \Phi_x + \Delta\Phi_x = \begin{bmatrix} 1 & -x\frac{d\alpha}{dx} & x\frac{d\beta}{dx} & x(1+\delta x) \\ x\frac{d\alpha}{dx} & 1 & -x\frac{d\gamma}{dx} & \frac{x^2}{2}\frac{d\alpha}{dx} \\ -x\frac{d\beta}{dx} & x\frac{d\gamma}{dx} & 1 & -\frac{x^2}{2}\frac{d\beta}{dx} \\ 0 & 0 & 0 & 1 \end{bmatrix}, \tag{5}$$

where x is the commanded joint position, δx is a rate of accumulation of positioning error and $d\alpha/dx$, $d\beta/dx$ and $d\gamma/dx$ are the rates of accumulation of angular errors (roll, pitch and yaw) as the joint moves along X-axis. The linear variation of angular errors with displacement along the axis necessitates the addition of squared terms to the straightness error. One may add additional higher order terms to account for other effects. Fig. 2(c) shows the relationships between the error terms and the fixed and moving coordinate frames for such a joint model. HTMs for inaccurate prismatic joints for Y, Z and W axes can also be derived.

2.4. Volumetric error model

Now combining all the HTMs of inaccurate joints and structural members defined in equations (2), (4) and (5), the actual coordinate transformation that takes a point on the tool expressed in the spindle frame to a frame attached

$$R = \Phi_B \,'T_1\,'\Phi_x\,'T_2\,'\Phi_z\,'T_3\,'\Phi_y\,'T_4\,'\Phi_w\,'T_5\,' \tag{6}$$

Eliminating second and higher-order terms of small errors, the first-order forward kinematic equation with errors for the machine can be written as:

$$R = H + \Delta H + O(2) \approx H + \Delta H, \tag{7}$$

where H is the ideal forward kinematics derived in equation (1), determined by ideal machine joints and nominal dimensions of the structural members that hold them (i.e., ideal joint and shape transformations) are given, ΔH is the sum of ten first-order terms, and $O(2)$ represents all higher order terms.

Thus, the machine's volumetric error components can be defined as the difference between actual and ideal forward kinematics,

$$\begin{bmatrix} \vec{e} \\ 1 \end{bmatrix} = T_0 \left(R - H \right) \begin{bmatrix} \vec{r}_t \\ 1 \end{bmatrix} \approx T_0 \Delta H \begin{bmatrix} \vec{r}_t \\ 1 \end{bmatrix}, \tag{8}$$

where $\vec{e}$ is the error vector $\vec{e} = \begin{bmatrix} e_x & e_y & e_z \end{bmatrix}^T$, T_0 is one additional shape transformation added to obtain a convenient reference for measurement or programming, and $\vec{r}_t$ is the position of the target in the spindle frame.

3. Identification of the error model parameters

The model, developed in the previous section, assembles all the error sources in the kinematic chain to obtain their influence on the volumetric error components of the machine. There are a total of 52 error sources or parameters (five shape transformations, each with six error parameters, four joint transformations for linear axes, each with four error parameters, and one for a rotary axis with six parameters) that are composed into an expression for the volumetric error components observed in the machines workspace. To use this model for compensating the volumetric errors, it is necessary to obtain values for these parameters.

Estimation of the parameters in the error model is done by observing the volumetric errors of the machine at different points in its workspace with a laser tracker, as shown in Fig. 3. However, to do so, the frame in which the laser tracker makes measurements, T_0 must be first estimated before the parameters of the error model can be obtained. *This is done* in the following two steps.

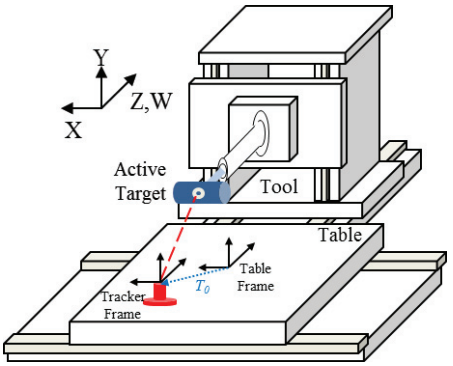

Fig. 3. Schematic depiction of measurement of volumetric error components of the machine using a laser tracker. The relationship between the measurement frame and the table frame (from the kinematic model of the machine) is captured by the homogeneous transformation matrix T_0.

3.1. Find T_0 , the best-fit measurement frame

Assume the machine to be ideal and identify the best values for T_0 to minimize the discrepancy between the laser tracker observations of position and the commanded position. Since T_0 is a rigid transformation, this step accounts any location and alignment errors between the machine and the laser tracker as shown in Fig. 3. In addition, this step will also reduce the effects of any error sources that produce a rigid displacement of the entire machines workspace. The residual errors that result from this process (of aligning measuring frame with the machines coordinates) are referred to as the nominal errors of the machine.

To identify T_0 , assume ideal kinematics for the machine defined in equation (1),

$$\vec{r}_{t0} = T_0 \Phi_B T_1 \Phi_x T_2 \Phi_z T_3 \Phi_y T_4 \Phi_w T_5 \vec{r}_t = T_0 H \vec{r}_t, \tag{9}$$

where T_0 has rigid body translations and small angle rotations as parameters to be identified.

$$T_0 = \begin{bmatrix} 1 & -\alpha_0 & \beta_0 & x_0 \\ \alpha_0 & 1 & -\gamma_0 & y_0 \\ -\beta_0 & \gamma_0 & 1 & z_0 \\ 0 & 0 & 0 & 1 \end{bmatrix}, \tag{10}$$

Further, $\vec{r}_t$ is the position of the target in the spindle frame and $\vec{r}_{t0}$ is its image in the measurement frame. For different joint commands (or measurement points), the kinematic transmission of the machine, H will vary. For the ith measurement point, the error vector, $\vec{e}_i$ between the forward kinematic transmission and the measurement recorded by the laser tracker can be expressed as

$$\vec{e}_i \equiv T_0 H_i \vec{r}_t - \vec{q}_i, \tag{11}$$

where $\vec{q}_i$ is the measurement recorded by the tracker. The best-fit homogeneous transformation, T_0 to the measurement frame can be obtained by minimizing the sum-of-squares of the discrepancy between the ideal machine's commanded positions and the measurements made by the tracker.

3.2. Identify the parameters of the error model from the nominal errors observed in the machine's workspace

The error sources in the kinematic chain of the machine cause the workspace of the machine to dilate/contract, shear and bend. These effects are encoded errors measured in the point-cloud of error measurements made by the laser tracker. In this step, least-square is used to identify the parameters.

As mentioned earlier, there are 52 error sources/parameters in the error model. Further, for the derivation of the error model, these errors are assumed to be small. The model is linear in the set of parameters and can be expressed by an error parameter vector, $\vec{p}$ pre-multiplied by a coefficient matrix, M

$$\vec{e} = M\vec{p}, \tag{12}$$

where $\vec{p}$ contains all 52 error parameters and M is a matrix with three rows and 52 columns, where each term being a function of known machine constants and commanded positions. Each row then represents the coefficients of the linear combination that take the error sources to the X, Y and Z components of volumetric error at a point in the machine's workspace.

As would be expected, the influence of some parameters on the observed volumetric error components will be inseparable from each other by only change the commanded position of the tool. For example, Δx_i and β_5 contribute in exactly the same manner to volumetric error components at a point, irrespective of its location in the machine's workspace. They must therefore be identified as a group. Further, other parameters such as α_4, α_5 and $d\alpha / dw$ will have no influence on the volumetric error when the tool reference point lies along the axis of the spindle. In all, our analysis has found that with such groupings and eliminations, there are 32 identifiable error parameters. After all these redundant parameters are eliminated or grouped, we have $\vec{e} = \mathsf{M}\ \vec{p}'$ where $\mathsf{M} \in \mathsf{R}^{3\times 32}$ is a sub-matrix of M and

$$\vec{p}' = [\alpha_1, \alpha_2 + \alpha_3, \beta_1, \beta_2, \beta_3 + \beta_4, \gamma_1 + \gamma_2, \gamma_3, \gamma_4, -\beta_5 r_t + \textstyle\sum_{i=1}^{5} \Delta x_i, \gamma_5 r_t + \sum_{i=1}^{5} \Delta y_i, \sum_{i=1}^{5} \Delta z_i, d\alpha / dx, d\beta / dx, d\gamma / dx, \delta x,$$
$$d\alpha / dy, d\beta / dy, d\gamma / dy, \delta y, d\alpha / dz, d\beta / dz, d\gamma / dz, \delta z, d\beta / dw, d\gamma / dw, \delta w, \alpha, \beta, \gamma, d_x, d_y, d_z]^T \in \mathsf{R}^{32}$$

The tool length is r_t. The M matrix for the above set of parameters, constructed for a particular point in the machines workspace, as previously mentioned, has elements made up of functions of the machine's constants and the axial commands that correspond to that point. Thus we have,

$$\vec{e} = \mathsf{M}\ \vec{p}' \; or \begin{bmatrix} e_x \\ e_y \\ e_z \end{bmatrix} = \begin{bmatrix} \mathsf{M}_x \\ \mathsf{M}_y \\ \mathsf{M}_z \end{bmatrix} \vec{p}', \tag{13}$$

where M_x, M_y and M_z correspond to the linear combinations of the error parameters that produce e_x, e_y and e_z.

Now if we consider an observation set consisting of errors observed at n points, under the assumption that the errors observed at each point, *i* is explained by the model

$$\vec{e}_i = \mathsf{M}_i \vec{p}' + \vec{N}, \tag{14}$$

where $\vec{e}_i = \begin{bmatrix} e_{x,i} & e_{y,i} & e_{z,i} \end{bmatrix}^T$ contains the components of the errors observed at that point, M_i is the corresponding 3x32 relational matrix and $\vec{N} \in \mathsf{R}^3$ is the observation noise vector with elements drawn from the Gaussian distribution $\mathrm{N}(0, \sigma)$, σ being the standard deviation of the observation noise, we can set up a system of 3n equations for estimating the parameters:

$$\boldsymbol{e} \approx \mathsf{M}\ \vec{p}', \tag{15}$$

where $\boldsymbol{e} = [e_{x,1}\ e_{y,1}\ e_{z,1} \ldots e_{x,n}\ e_{y,n}\ e_{z,n}]^T \in \mathbb{R}^{3n}$ vector containing the components of the measured error vectors in the point-set, $\mathbf{M} = \left[\mathrm{M}_1^T \ldots \mathrm{M}_n^T\right]^T$ is the new coefficient.

The least-squares estimate of $\vec{p}'$ which minimizes the sum of squares of the discrepancy between the RHS and LHS of equation (15) is given by:

$$\hat{p} = (\mathbf{M}^T\mathbf{M})^{-1}\mathbf{M}^T\boldsymbol{e} \tag{16}$$

The estimate $\hat{p}$ minimizes the L_2-norm of the residuals, $\|\boldsymbol{e} - \mathbf{M}\ \vec{p}'\|_2 \equiv (\boldsymbol{e} - \mathbf{M}\ \vec{p}')^T(\boldsymbol{e} - \mathbf{M}\ \vec{p}')$ and produces an unbiased estimate of $\vec{p}'$ over the entire set of observations (and the workspace, if the point-set is a good representation of it).

4. Experimental Results

4.1. Data Collection

In order to identify the kinematic error model parameters, measurements of the machine tool are taken. These measurements are collected over the entire 3D space using a Laser Tracker and Active Target system (Fig. 4(a)) to ensure that all axis-dependent machine tool geometric errors are captured. The Laser Tracker used in this test is the API Radian which has a static measurement accuracy of 5 ppm (2σ) according to the specifications provided by API. From this and the tracker's position on the machine, the largest measurement standard deviation (σ) value over the measured range was calculated to be 8.9 μm. In order to ensure that the Laser Tracker was thermally isolated from the machine tool, a plastic Isolation Block was placed between the Laser Tracker base and the machine tool.

Before measurements are taken, a measurement frame is identified. With the Laser Tracker attached to the machine tool bed and the Active Target attached to the machine tool spindle, as shown in Fig. 4(a), the B-Axis is rotated with the other axes stationary in order to generate a circle of points. The normal vector of this circle is used as the vertical (Y-Axis) of the measurement frame. Next, the B-Axis is re-oriented to its 0° position and three points are measured as the machine moves along its X-Axis. The best fit line to these points is used as the X-Axis direction of the measurement frame. A right-handed frame is established from these two axes. This frame is then transformed into the negative Y-Axis direction by the Y-Axis encoder value of the machine tool in order to account for the Y position of the machine tool spindle during the measurement frame identification.

The machine tool repeatability, which establishes the maximum possible accuracy for a perfectly compensated machine tool, was calculated next. In order to determine the machine tool's repeatability, eight quasi-random points from the machine tool's working joint space were measured ten times each. Each cycle of the eight points was

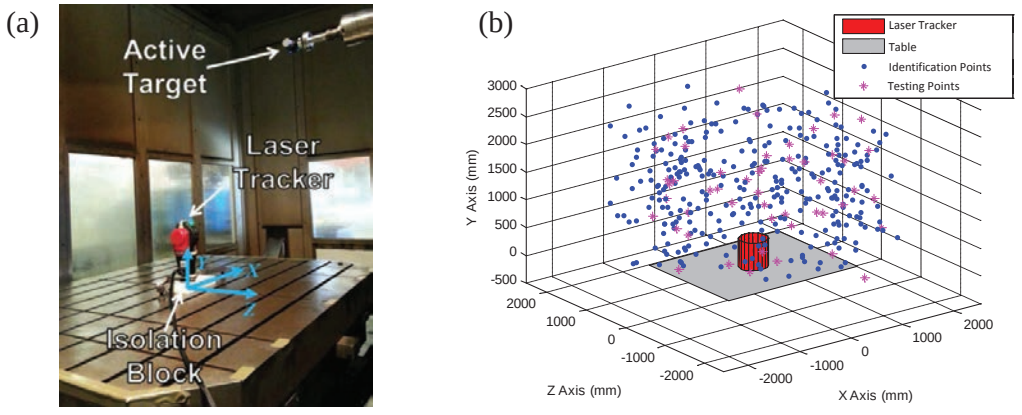

Fig. 4(a). Machine tool work cell and table base frame; (b) Positions of identification and testing points inside working envelop, given in machine tool base frame.

measured in a different randomized order to approximate arbitrary approach directions. The error of each measurement is

$$e_{i,j} = \sqrt{\left(x_{i,j} - \bar{x}_i\right)^2 + \left(y_{i,j} - \bar{y}_i\right)^2 + \left(z_{i,j} - \bar{z}_i\right)^2}, \tag{17}$$

where $e_{i,j}$ is the error of the j^{th} measurement of the i^{th} point, $[x_{i,j}, y_{i,j}, z_{i,j}]$ is the j^{th} measurement of the i^{th} point, and $[\bar{x}_i, \bar{y}_i, \bar{z}_i]$ is the average measurement of the i^{th} point. From the measurements taken of the machine, the largest error was 0.0217 mm, which is used as the machine tool's repeatability. It should be noted that this repeatability value is only 2.4 times the measurement standard deviation meaning that a large portion of this value is may be due to the accuracy level of the laser tracker as opposed to the machine itself. Despite this fact, this repeatability still corresponds to the highest potential measured accuracy of the machine if it was perfectly compensated.

The measurement locations used for model identification and testing were selected next. For the identification set, 290 quasi-random points were selected throughout the machine tool's joint space, and an additional 50 quasi-random points were generated as a testing set. The number of points selected for identification and testing was selected through past experience with similar sized machine tools [25]. This number has the necessary richness to appropriately identify the geometric errors of the machine tool while minimizing the machine tool's down time. The joint ranges used to generate these points are shown below in Table 1, and the distributions of the points are shown below in Fig. 4(b).

Table 1: Minimum and maximum commands used for modeling and testing.

Axis	Minimum Command	Maximum Command
B	0°	360°
X	-1250 mm	1250 mm
Z	900 mm	2200 mm
Y	350 mm	2500 mm
W	-800 mm	-200 mm

Using the Laser Tracker and Active Target system, the 290 point identification set was measured twice. In each measurement set a different length mount was used to attach the active target to the spindle as shown in Fig. 4(a). Because the rotation of the spindle does not need to be modeled, these two mounts (Fig. 5(a)) allow for the spindle orientation to be determined for each point by finding the vector between the measurement sets.

Because the same axis commands are used when taking both sets of identification points, it is possible to use the two sets of measurements to examine the potential existence of thermal drift in the measurement setup. For each point in the identification set, the distance between the two measurements of that point is ideally equal to the tool length difference of the two Active Target mounts (within machine tool repeatability). Therefore, if the distance

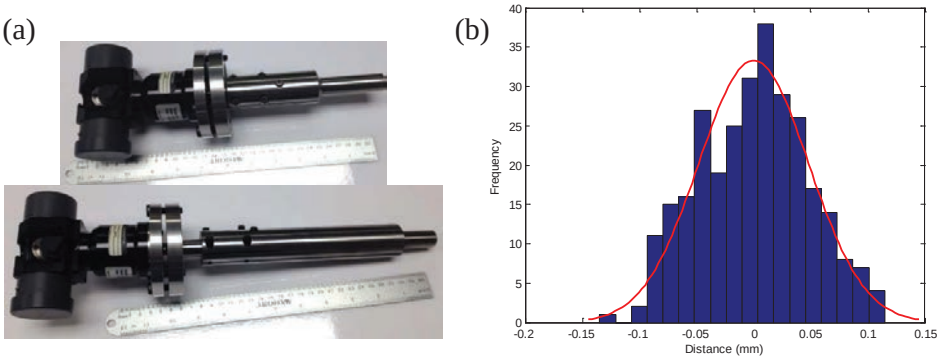

Fig. 5(a). Active Target machine tool spindle mounts; (b) Distance between short tool and long tool measurements.

between measurements is larger than the repeatability (0.0217 mm), then some shift must have occurred during the time that the system was measured. The distances between the measurements from each set (with the tool length offset removed) are shown in Fig. 5(b). The distance between corresponding points ranges from -0.13 to 0.11 mm. Since this value is approximately six times the measured repeatability value, there is evidence that some sort of drift occurred during the measurement process. Furthermore since the air temperature changed by 3.7°C during the measurement process, thermal effects is a likely source of some or all of this drift.

4.2. Best-Fit Measurement Frame

The procedure described in Sec. 3.1 was used on the data collected in both the identification and testing data sets (described in Sec. 4.1). Table 2 shows the estimated errors between the nominal measurement frame and the machine's reference. Also shown in the table is the mean magnitude of the residual error vectors at the measurement points. For identification purpose, two sets of measurement were taken using different lengths of tool. After that, the identified parameters were used for modeling the testing sets.

Table 2: Best measuring frames of each measuring set.

Set	Short Tool	Long Tool	Test 1	Test 2
x_0(mm)	0.00845	0.0122	0.00715	0.0111
y_0(mm)	0.351	0.304	0.293	0.298
z_0(mm)	-0.0147	-0.0124	0.0095	0.0116
α_0(rad)	-6.21E-06	3.68E-05	5.78E-05	6.68E-05
β_0(rad)	-2.13E-05	-1.85E-05	-2.43E-05	-2.35E-05
γ_0(rad)	1.05E-05	2.41E-05	3.52E-06	5.05E-06
Res(mm)	0.4214	0.3175	0.2783	0.2745

4.3. Parameter Identification

The results of parameter identification are shown in Table 3. The data for the two different tools (short, 312.035mm, and long, 435.185mm) were analyzed separately to identify the error parameters of the two identification sets. From Table 3, the high correlation between the parameters identified in the two experiments is apparent. The deviations seen are due to the temperature changes between the two experiments and the uncertainty in the assembly of the target on the tool. Fig. 6(a) shows the distributions of the residual errors. The statistical

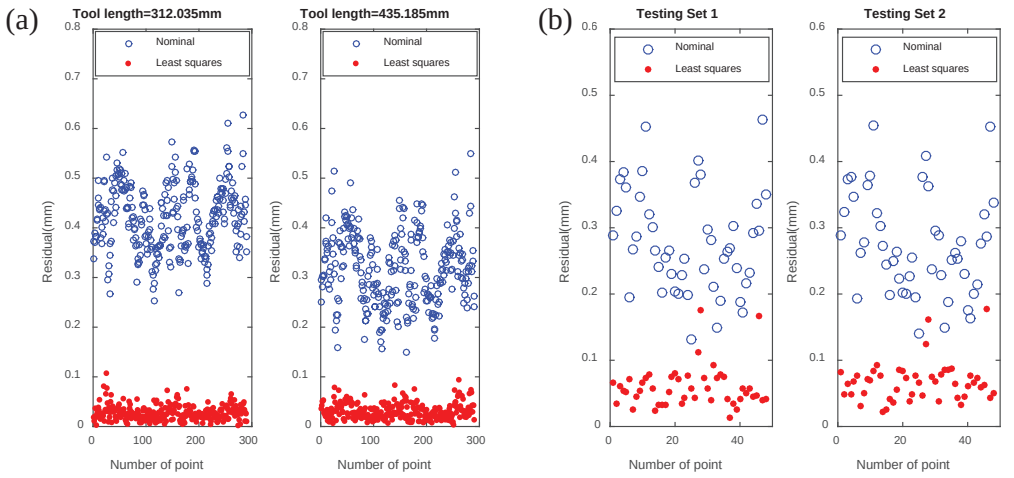

Fig. 6(a). The magnitudes of error residuals on two identification sets (290 points in each); (b) the magnitudes of error residuals on two testing sets (48 points in each).

analysis of the results is shown in Table 4. Compared with the residual errors obtained from the frame alignment process, the error model reduces not only the mean but also the maximum (which characterizes the worst-case uncertainty of the machine/model) errors by 90% and 82% respectively.

Table 3: Values identified for the parameters of the error model.

Unit: mm			Unit: rad			Unit: rad/mm		
Parameter	Short	Long	Parameter	Short	Long	Parameter	Short	Long
$x_1+\ldots x_5-t_1\beta_5$	3.62E-02	5.92E-02	α_1	-2.36E-05	-1.96E-05	$d\alpha/dx$	1.55E-08	2.57E-08
$y_1+\ldots y_5+t_1\gamma_5$	-4.78E-02	-2.35E-02	$\alpha_2+\alpha_3$	-1.01E-05	-1.18E-05	$d\beta/dx$	1.13E-09	7.01E-09
$z_1+\ldots z_5$	-3.12E-01	-1.97E-01	β_1	-6.93E-05	-6.95E-05	$d\gamma/dx$	-1.04E-08	-1.16E-08
dx	1.13E-02	3.75E-03	β_2	4.16E-05	3.51E-05	$d\alpha/dy$	-1.26E-08	-1.80E-08
dy	2.62E-02	2.71E-02	$\beta_3+\beta_4$	5.83E-05	4.82E-05	$d\beta/dy$	2.57E-08	3.03E-08
dz	-1.28E-02	-7.25E-03	$\gamma_1+\gamma_2$	-1.85E-04	-1.77E-04	$d\gamma/dy$	-5.54E-09	-1.54E-09
Unit: dimensionless			γ_3	9.02E-05	8.19E-05	$d\alpha/dz$	-1.68E-08	-1.34E-08
Parameter	Short	Long	γ_4	-1.85E-04	-2.07E-04	$d\beta/dz$	-3.81E-08	-2.73E-08
δx	-1.23E-04	-1.12E-04	β	-9.57E-07	-9.72E-06	$d\gamma/dz$	2.97E-08	2.78E-08
δy	-1.10E-04	-1.09E-04	α	1.15E-06	6.78E-07	$d\beta/dw$	2.93E-08	1.80E-08
δz	-3.75E-05	-3.75E-05	γ	8.03E-06	4.84E-06	$d\gamma/dw$	-4.10E-07	-4.19E-07
δw	-1.06E-04	-1.06E-04						

Table 4: Model performance for two sets with two different tool lengths.

Tool length=312.035mm	Mean Residual	% decrease	Max. Residual	% decrease
Nominal	0.4214 mm	N/A	0.6270 mm	N/A
Least squares	0.0277 mm	93.43%	0.1073 mm	82.88%
Tool length=435.185mm	Mean Residual	% decrease	Max. Residual	% decrease
Nominal	0.3175 mm	N/A	0.5492 mm	N/A
Least squares	0.0307 mm	90.34%	0.0941 mm	82.86%

4.4. Model Testing

With the error model parameters obtained from the identification sets, the model's prediction capability are checked against two testing sets consisting of 48 previously-unseen data points, taken with the long tool. The results of this testing are shown in Table 5 and Fig. 6(b). Compared with the nominal machine errors, the model is able to provide, approximately, a 75% reduction of average magnitude of errors vectors at the points in the data sets.

Table 5: Model performance for two testing data sets (Tool length=435.185mm).

Testing set 1	Mean Residual	% decrease	Max. Residual	% decrease
Nominal	0.2783 mm	N/A	0.4624 mm	N/A
Least squares	0.0590 mm	78.80%	0.1760 mm	61.94%
Testing set 2	Mean Residual	% decrease	Max. Residual	% decrease
Nominal	0.2745 mm	N/A	0.4546 mm	N/A
Least squares	0.0670 mm	75.59%	0.1767 mm	61.13%

4. Summary and Conclusions

This paper has developed a kinematics model for a 5-axis machine tool with a redundant linear axis. This model introduced 52 parameters, linked to the error kinematics of the machine-tool, which would need to be identified. Analysis of the model shows that only 32 of them have linearly independent effects on the volumetric errors in the workspace. Procedures for least-squares identification of the error model parameters from observations of the volumetric errors at points in the machine's workspace are developed in this paper.

A laser tracker was used to make measurements at 290 randomly generated points in the machine's workspace. These measurements were repeated with tools of two different lengths characterizing the behavior of the machine with long and short tools. The error model parameters were estimated for these two different data sets. In spite of some thermal drift on the machine between the experiments, the error model parameters estimated remained consistent in both magnitude and sign. Further, the model was able to reduce the errors at the observation points to about a third of their original values. The model was tested on two data sets of 48 observation points each. A similar model performance was observed. The proposed model could be used for error prediction on commanded positions.

The average magnitude of residual error vectors in the training sets were about 30 microns. This is consistent with the repeatability of the machine and the fact that the thermal environment changed during the experiments. The modeling approach, along with the convenience of observing errors as a large set of randomly selected points in a machine's workspace with a laser tracker can make for a very effective means of regularly updating compensation tables of machines.

For better model performance, a thermally stable environment would be necessary. Additionally, tracking the thermal drift of the machine with time would yield better model performance. For this, a quicker (consisting of fewer and more strategically-chosen points) and more convenient data-collection cycle that can be easily embedded into the normal operation of the machine is needed. A higher order model that better describes machine's error characteristic is another approach to reduce the modeling residual.

Acknowledgements

This work was performed with support from the Digital Manufacturing and Design Innovation Institute (DMDII) under project DMDII14-07-02: Integrated Manufacturing Variation Management. The project is sponsored in part by the Department of Army. The authors would also like to acknowledge inputs and supports from Nien Lee, Richard Eirhart, Keith Egland, Mike Vogler and Craig Habeger of Caterpillar Inc. and Jorge E. Correa of UIUC.

References

[1] Ferreira, P. M., & Liu, C. R., 1993. A method for estimating and compensating quasistatic errors of machine tools. Journal of Engineering for Industry, 115(1), 149-159.
[2] Kiridena, V. S. B., & Ferreira, P. M., 1994. Kinematic modeling of quasistatic errors of three-axis machining centers. International Journal of Machine Tools and Manufacture, 34(1), 85-100.
[3] Yang, S., Yuan, J., & Ni, J., 1996. Accuracy enhancement of a horizontal machining center by real-time error compensation. Journal of Manufacturing Systems, 15(2), 113-124.
[4] Rahman, M., Heikkala, J., & Lappalainen, K., 2000. Modeling, measurement and error compensation of multi-axis machine tools. Part I: theory. International Journal of Machine Tools and Manufacture, 40(10), 1535-1546.
[5] Ramesh, R., Mannan, M. A., & Poo, A. N. 2000. Error compensation in machine tools—a review: Part II: thermal errors. International Journal of Machine Tools and Manufacture, 40(9), 1257-1284.
[6] Aguado, S., Samper, D., Santolaria, J., & Aguilar, J. J., 2012. Identification strategy of error parameter in volumetric error compensation of machine tool based on laser tracker measurements. International Journal of Machine Tools and Manufacture, 53(1), 160-169.
[7] Ramesh, R., Mannan, M. A., & Poo, A. N. 2000. Error compensation in machine tools—a review: part I: geometric, cutting-force induced and fixture-dependent errors. International Journal of Machine Tools and Manufacture, 40(9), 1235-1256.
[8] Ferreira, P. M., & Liu, C. R., 1986. An analytical quadratic model for the geometric error of a machine tool. Journal of Manufacturing Systems, 5(1), 51-63.
[9] Suh, S. H., Lee, E. S., & Jung, S. Y., 1998. Error modelling and measurement for the rotary table of five-axis machine tools. The International Journal of Advanced Manufacturing Technology, 14(9), 656-663.
[10] Okafor, A. C., & Ertekin, Y. M., 2000. Derivation of machine tool error models and error compensation procedure for three axes vertical machining center using rigid body kinematics. International Journal of Machine Tools and Manufacture, 40(8), 1199-1213.

[11] Kiridena, V. S., 1993. Modeling, parameter estimation and compensation of quasistatic errors in multi-axis CNC machining centers (Doctoral dissertation, University of Illinois at Urbana-Champaign).
[12] Sheth, P. N., & Uicker, J. J. 1971. A generalized symbolic notation for mechanisms. Journal of Engineering for Industry, 93(1), 102-112.
[13] Denavit, J. 1955. A kinematic notation for lower-pair mechanisms based on matrices. Trans. of the ASME. Journal of Applied Mechanics, 22, 215-221.
[14] Schwenke, H., Franke, M., Hannaford, J., & Kunzmann, H. 2005. Error mapping of CMMs and machine tools by a single tracking interferometer. CIRP Annals-Manufacturing Technology, 54(1), 475-478.
[15] Schwenke, H., Schmitt, R., Jatzkowski, P., & Warmann, C. 2009. On-the-fly calibration of linear and rotary axes of machine tools and CMMs using a tracking interferometer. CIRP Annals-Manufacturing Technology, 58(1), 477-480.
[16] Patel, A. J., & Ehmann, K. F. 1997. Volumetric error analysis of a Stewart platform-based machine tool. CIRP Annals-Manufacturing Technology, 46(1), 287-290.
[17] Ferreira, P. M., Liu, C. R., & Merchant, E. 1986. A contribution to the analysis and compensation of the geometric error of a machining center. CIRP Annals-Manufacturing Technology, 35(1), 259-262.
[18] Kiridena, V., & Ferreira, P. M. 1993. Mapping the effects of positioning errors on the volumetric accuracy of five-axis CNC machine tools. International Journal of Machine Tools and Manufacture, 33(3), 417-437.
[19] Yuan, J., & Ni, J. 1998. The real-time error compensation technique for CNC machining systems. Mechatronics, 8(4), 359-380.
[20] Ni, J. 1997. CNC machine accuracy enhancement through real-time error compensation. Journal of manufacturing science and engineering, 119(4B), 717-725.
[21] Donmez, M. A., Blomquist, D. S., Hocken, R. J., Liu, C. R., & Barash, M. M. 1986. A general methodology for machine tool accuracy enhancement by error compensation. Precision Engineering, 8(4), 187-196.
[22] Wang, S. M., & Ehmann, K. F. 2002. Error model and accuracy analysis of a six-DOF Stewart platform. Journal of manufacturing science and engineering, 124(2), 286-295.
[23] Creighton, E., Honegger, A., Tulsian, A., & Mukhopadhyay, D. 2010. Analysis of thermal errors in a high-speed micro-milling spindle. International Journal of Machine Tools and Manufacture, 50(4), 386-393.
[24] Veldhuis, S. C., & Elbestawi, M. A. 1995. A strategy for the compensation of errors in five-axis machining. CIRP Annals-Manufacturing Technology, 44(1), 373-377.
[25] Creamer, J. R., Sammons, P. M., Bristow, D., Landers, R. G., Freeman, P., & Easley, S. 2013, November. Table-Based Compensation for 5-Axis Machine Tools. In ASME 2013 International Mechanical Engineering Congress and Exposition (pp. V02AT02A071-V02AT02A071). American Society of Mechanical Engineers.